R07-29

A Sodar Height Sensor for Precision Airdrops

Anthony Dietz and Paul Sorenson
Creare Inc, Hanover, NH, 03755, USA

Ken Steele
Kaman Aerospace Corporation, Tuscon, AZ, 85742, USA

and

Kristen Lafond and Steve Tavan
US Army Natick Soldier Research, Development and Engineering Center, Natick, MA, 01760, USA

Abstract: Accurate estimations of the height and velocity of precision airdrop systems are required to control final deceleration maneuvers. Airdrop systems have a limited deceleration window, so robust and reliable estimations are required. Radar, sodar, and lidar sensors have been evaluated for this role with varying degrees of success. Foliage and vegetation prove troubling for many of the sensors. However, sodar has been shown to successfully penetrate ground vegetation at certain frequencies. The development and testing of a Sodar Height Sensor (SHS) for precision airdrop applications is reported in this paper. The SHS incorporates a speaker, a microphone, a barometer, and temperature sensors. Estimation algorithms running on a Digital Signal Processor (DSP) produce continuous estimates of the sensor height above ground. The sensor's performance has been characterized in a series of laboratory, field, and airdrop tests. The sensor range can be greater than 1000 ft depending on the mounting location while its accuracy approaches a one-foot tolerance as the sensor approaches the ground.

I. Introduction

Precision airdrop systems have the potential to transform resupply operations by delivering payloads accurately from a safe height and offset distance to small distributed drop zones. A number of guided parafoil systems have already been fielded and further systems are currently being developed. These systems include an Airborne Guidance Unit (AGU) that uses GPS information to control the drop trajectory. While, GPS-based control is sufficient for most of the flight, the uncertainty of GPS height information results in unacceptable overshoots and undershoots in the direction of travel as well has high impact velocities due to mistimed landing flares. A robust, reliable and accurate height sensor is required so that the final deceleration maneuvers may be precisely timed. To be useful in this application, the height sensor accuracy should approach ± 1 foot as it nears the ground and the sensor must be able to penetrate smoke, fog, dust, rain, or snow, and not be confused by ground vegetation or be corrupted by acoustic and electromagnetic interference. The development and testing of a Sodar Height Sensor (SHS) that meets these requirements is described in this paper. The sensor concept was initially described by Ulich et al. (2003).

II. Choice of Sensing Modality

A. Sensor

Barometric altimeters are typically used as the primary height sensor in aircraft. However, the barometric pressure at the drop zone will not be known by autonomous airdrop systems. So while a barometric pressure sensor may give accurate measurements of relative altitude and descent rate, there is no way to determine the absolute height above ground.

Radar (radio detection and ranging), lidar (light detection and ranging), and sodar (sound detection and ranging) sensors are alternative approaches, where the time of flight of a wave pulse transmitted towards the ground is used

to determine height. However, foliage and ground vegetation prove particularly challenging for the short-wavelength sensing modalities such as radar, lidar and ultrasonic sodar. When the wavelength of the transmitted pulse is small compared to the characteristic length of the vegetation, the primary return will be from the upper surface of the vegetation. Systems with small wavelengths must then rely on the use of multiple frequencies or the detection of highly attenuated last return signals for vegetation penetration.

When the wavelength of the transmitted pulse is comparable to or larger than the vegetation, the waves will penetrate the vegetation, diffracting and scattering around the foliage. In these cases the primary return will be from the ground. A Sodar sensor operating in the audible sound range has wavelengths suitable for vegetation penetration. This has been confirmed by studies on the propagation of bird song in forests (Price et al., 1988; Padgham, 2004) and others on the use of foliage for traffic noise abatement (Martens 1980). Furthermore, the sodar approach enables the use of mass-produced acoustic components, lowering the unit cost and facilitating integration into a small, lightweight, and robust unit.

B. Transmitted Waveform

The choice of sound transmission frequency is a trade between attenuation and sensor size. Directional high-frequency signals can be generated with small speakers. Directionality is important to minimize the region over which the sound is broadcast and to reduce interference between systems descending in close proximity. However, these waves suffer higher attenuation in the atmosphere and in foliage. Lower frequency waves suffer less attenuation, but require large speaker diaphragms and directional horns. A folded horn can reduce the length required for adequate directionality, but the opening diameter remains a fixed fraction of the transmitted wavelength. Taking these factors into consideration, a transmission frequency centered at 3 kHz was selected.

The duration of the transmitted wave pulse is another important variable. With a single frequency sound pulse the signal to noise ratio (SNR) of the ground return is proportional to the length of the pulse. Conversely, the height resolution is inversely proportional to the length of the pulse. This results in a trade between range and resolution. This problem may be addressed using an adaptive sounding technique where the pulse duration is decreased as the sensor approaches the ground. Another solution is pulse compression, a common technique used in radar and sonar applications to increase resolution without reducing SNR. One implementation is a linear frequency modulated (LFM) waveform (or chirp). When the return is processed through a matched filter, its resolution is dependant only on the bandwidth (swept frequency range) of the signal, while the SNR is dependant only on the pulse duration.

Sensor range is maximized by maximizing the initial amplitude of the transmitted pulse, and by minimizing the return signal detection threshold.

III. Sensor Design

A functional diagram of the SHS components is shown in Figure 1. The SHS incorporates five transducers: a speaker, a microphone, a pressure sensor, and two temperature sensors.

A. Sound Generation

Sensor range is maximized by maximizing the initial amplitude of the transmitted pulse. An efficient technique for producing very loud sound levels is to use a resonant piezoelectric speaker driver comprising a piezo-electric crystal bonded to a diaphragm mounted over a resonant cavity. A horn is added to improve the efficiency of the energy transmission from the speaker to the atmosphere by improving the acoustic impedance match between the two. The horn also improves the directionality of the transmitted sound. The piezo-electric driver requires a high-voltage AC signal. The required driving voltage is generated by a transformer that steps up the battery voltage. The desired waveform is generated by a switching circuit between the battery and the primary side of the transformer. The switching frequency is controlled by a digital signal from the Digital Signal Processor (DPS) providing a software configurable waveform. With this implementation, sound levels approaching 130 dB may be obtained. Despite the resonant nature of the speaker driver, the speaker bandwidth is sufficient to produce the desired resolution of 1 ft with a LFM signal.

B. Return Detection

The sensor range is also dependent on the threshold of detection of the return signal. This turns out to be less dependent on the sensitivity of the microphone than on the environmental noise at the sensor location from sources such as the wind, the payload, the AGU or the parachute. As much of this noise is at low frequencies, a bandpass

filter is used to reject noise outside the frequency range of interest prior to digital conversion. Microphone resistance to environmental noise is further improved by increasing its directionality by mounting it within the speaker horn. With this implementation the microphone must be able to survive the high sound level produced by the speaker while still retaining sufficient dynamic range to detect the return.

C. Atmospheric Data

A temperature sensor positioned in the air stream is used to provide measurements of the local air temperature. This temperature is used to determine the local speed of sound, which is needed to convert the time of flight measurements into height estimates. A pressure sensor mounted on the sensor circuit board provides measurements of the local static air pressure. A second temperature sensor, also located on the circuit board, is used to calibrate for any temperature sensitivity in the pressure sensor response. The pressure measurements are used to compute the descent velocity, which is used in the detection algorithm to reject false returns and also in the height estimation algorithm to account for the change in height of the sensor during the time of flight of the acoustic signal.

D. Other Components

Sensor processing and control operations are performed through algorithms running on a Digital Signal Processor (DSP). Four separate Analog Interface Circuits (AICs) are used to interface with the microphone and the temperature and pressure sensors. The sensor circuit includes additional volatile memory that is used for buffering during processing tasks, and non-volatile memory for the storage of program files and calibration constants. A wireless serial interface is included for communication of the pressure altitude, descent velocity and height above ground readings to the airdrop system's guidance unit. The sensor may also be programmed over this interface. Power is provided by a rechargeable NiMH battery pack. A latched lanyard switch is inserted between the battery and the circuit board so that the sensor will not be activated until it exits the aircraft.

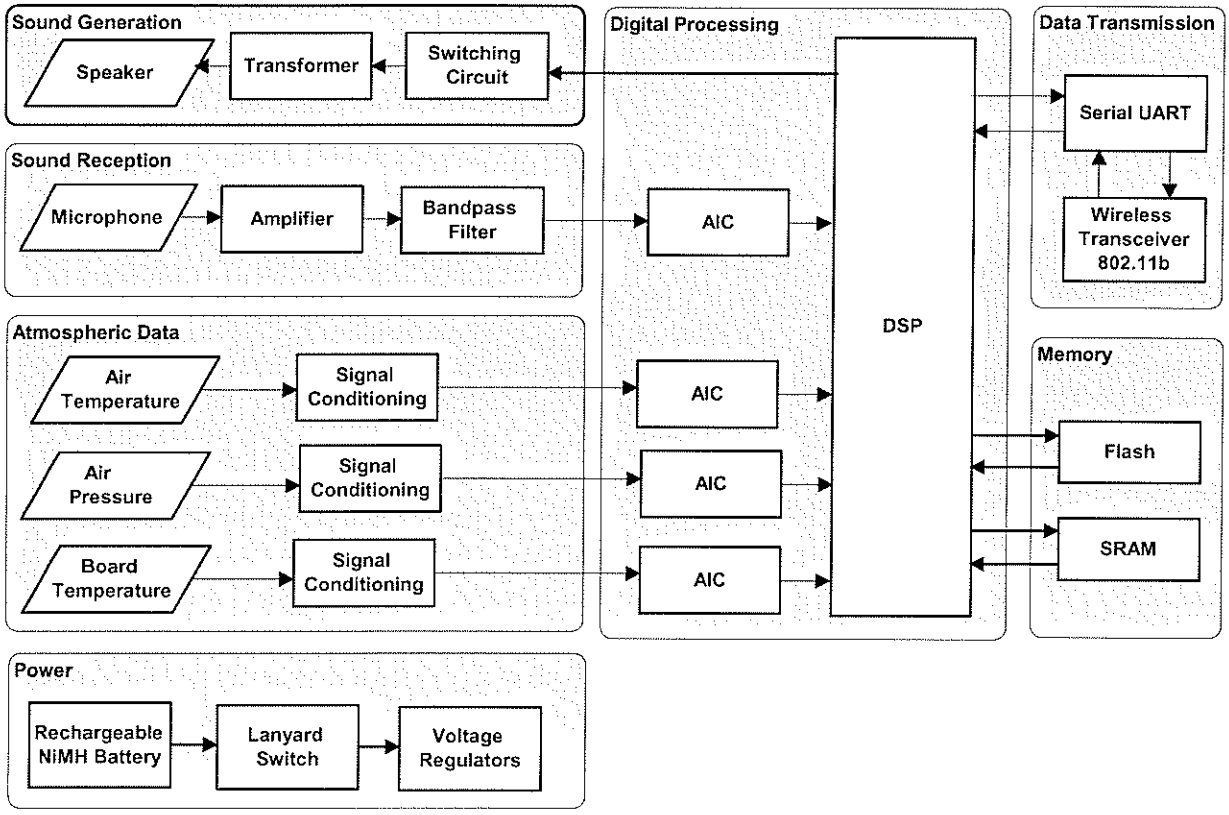

Figure 1. Sensor Functional Diagram.

IV. Algorithms

A. Waveform Transmission

Prior to each sounding, an adaptive altitude-dependent transmission algorithm computes the waveform to be transmitted by the sensor and the matched filter to be used to detect the return. The matched filter is adjusted to account for the Doppler frequency shift resulting from the sensor descent rate. The descent rate determined during the previous sounding is used. Initial transmissions are of long period chirp waveforms with a listening period that is greater than the maximum range of the sensor (1000 ft). This prevents the height ambiguities that might result from shorter sampling periods where the returns from previous transmissions may be detected. An alternative approach would be to use GPS height to resolve ambiguities. When the sensor determines that the height has passed a certain threshold, the listening period is reduced and estimates are reported at a higher rate. When the sensor determines it has passed a still lower threshold, the transmission waveform is changed to a short duration tone, which produces sufficient SNR at low heights and has a lower minimum detection height.

B. Detection Algorithm

The signal from the microphone is acquired for a period after each sound transmission and processed through the matched filter to produce potential ground returns. There is a dead period that extends some time after each transmission before microphone acquisition begins to prevent the inadvertent detection of signal artifacts associated with the ring down of the transducer following the pulse transmission. This dead period is dependent on the length of the pulse transmission and defines a minimum detection height for each waveform type. Following the dead period, the microphone signal is received and processed through the matched filter. The narrow-band filter returns are compared to a wide-band guard filter that is notched to reject the transmitted frequency. If both filters simultaneously produce a high return it is rejected as a wide-band noise event. If the matched filter return is high and the guard filter is low, then the time is retained as a 'raw detection.' For each sounding, the raw detections are sorted according to their SNR and a subset is retained for further processing.

C. Height Estimation Algorithm

Each of the raw detection times are converted to heights using Equation (1).

$$h = \frac{(a+V)\Delta t}{2} \qquad (1)$$

$$a = \sqrt{\gamma RT} \qquad (2)$$

$$V = \frac{RT\Delta P}{gP\Delta T} \qquad (3)$$

where h is the estimated height above ground at the beginning of the sound transmission; Δt is the detection time; a is the speed of sound determined from the measured air temperature T according to Equation (2), where γ is the adiabatic index and R is the gas constant; and V is the descent rate from Equation (3), where g is gravity and P is the measured air pressure.

D. Valid Ground Detections

Two heuristic rules are then used to further reject false detections. The first rule checks to see if any of the raw detections line up with any two raw detections from the previous five soundings along a trajectory that is within a specified tolerance of the descent rate V computed from the pressure transducer. The second rule then checks that the linearity of the trajectory defined by these three detections is within a second tighter tolerance. If this is the case, the detection is accepted as a valid ground detection. If there are multiple detections accepted from a single sounding, the detection with the highest SNR is accepted.

The performance of the ground detection algorithms is illustrated by the data plotted in Figure 2. The algorithms and heuristic rules combine to effectively eliminate all false positives and capture all of the true ground returns. Note that the first ground estimate is not reported until after the third sounding.

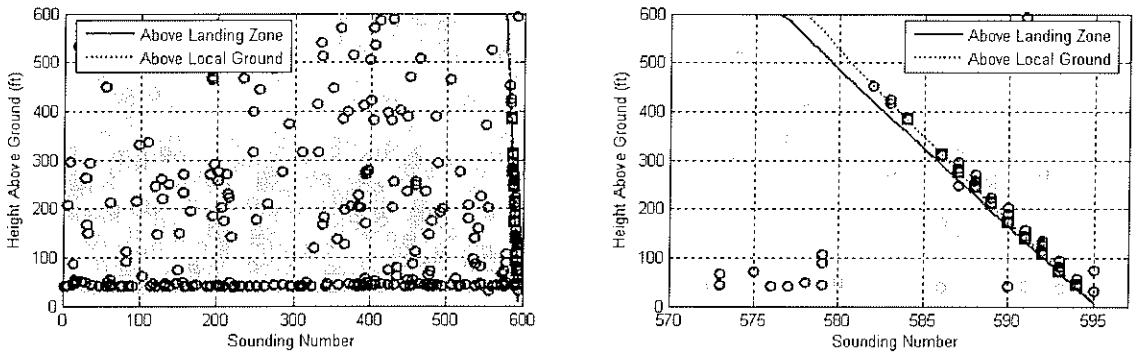

Figure 2. Height Estimation Process. The circles represent all of the detections that pass the matched filter. The light blue circles are those rejected through a comparison with the guard filter and the dark blue circles are retained as raw detections. The black squares are those detections that pass the heuristic rules and are reported as height above ground estimates.

V. Prototype Sensor

E. Sensor Construction

The sensor must be rugged to survive the stresses of airdrop operations. The initial implementation concept was for the sensor to be mounted in the AGU, which is typically suspended between the load and the parafoil. With this implementation, the sensor would be protected by the AGU housing and it would be spared large landing shocks. However, as discussed in a later section, poor sensor performance in the AGU resulted in sensor being moved to the load, where the environmental noise is lower and the sensor has a clear view of the ground. As the loads can hit the ground hard and often roll or are dragged along, the sensor packaging had to be very rugged. The final sensor prototype design is shown in Figure 3. The sensor is built up in a modular stack within a removable stainless steel enclosure. The modular structure is supported by four threaded rods that allow the position of each module in the stack to be adjusted. The speaker module is mounted in the base and protected by a grill. Foam is inserted behind the grill to reduce wind noise. The battery pack is mounted above the speaker module. It is designed to be recharged via the lanyard connector but it may be removed from the side if necessary without affecting any of the other components. The circuit board is mounted above the battery pack using shock isolation mounts. All connections to the board are made with positive locking connectors so that the board may be swapped out if necessary during field repairs. Uppermost is the connector plate, which holds the lanyard connector, the activation switch and the wireless antenna. The plate has a rubber gasket to ensure a weatherproof seal. The diameter of the sensor prototype is 5 inches and its height is 10 inches. The weight of the sensor prototype is 3.5 lbs.

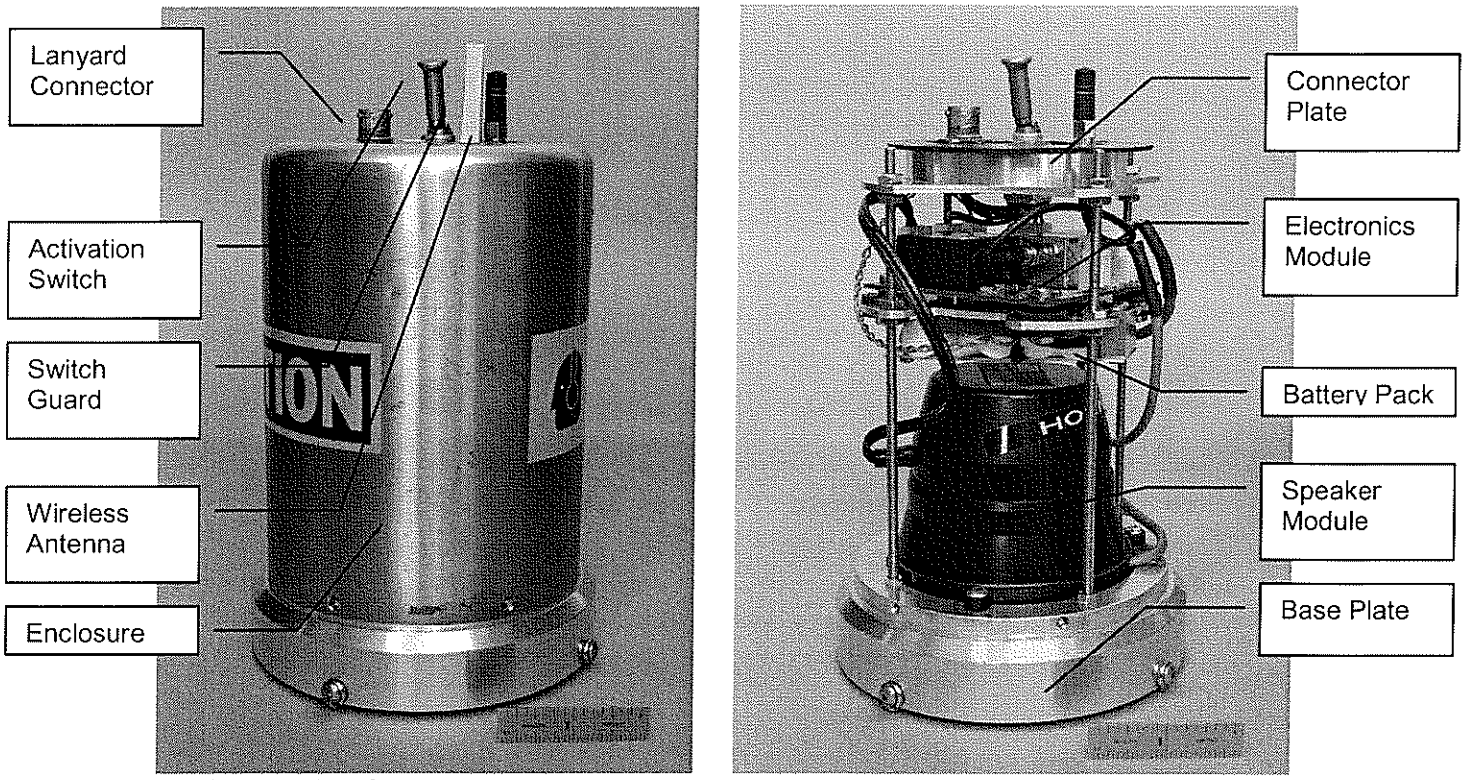

Figure 3. Sodar Height Sensor Prototype.

F. Sensor Mounting

The sensor is designed to be mounted vertically on the side of the load with the speaker pointing down so that it has a clear view of the ground. The mounting method must be flexible so that the sensor can be used with a wide variety of loads of different sizes, weights, compositions and restraint techniques. The mounting technique chosen is to attach a mounting bracket to the sensor using a hose clamp. Tie down straps are then threaded through the mounting bracket and looped around the load for small loads, or else looped around adjacent load restraint straps on large loads. The straps are then cinched down to lock the sensor in position. An example mounting is shown in Figure 4. While the mounting method is still being refined, the sensor has been drop tested on a number of different loads as reported in the following section with good success.

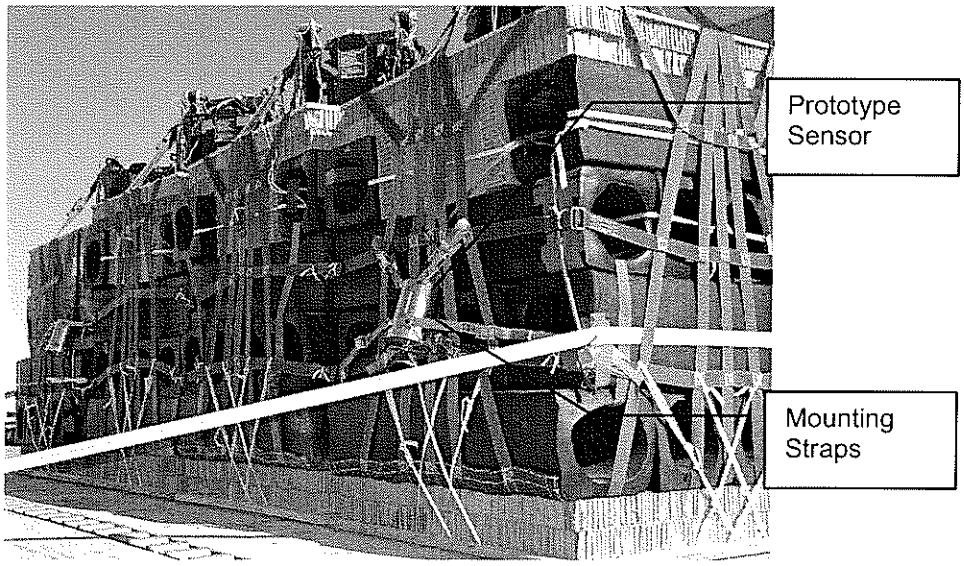

Figure 4. Sensor Mounting Technique. Creare Sensor Prototype shown mounted on a Sherpa load prior to airdrop testing at YUMA.

VI. Sensor Performance Testing

A. Vegetation Penetration

The vegetation penetration characteristics of the sodar sensor were evaluated by suspending the sodar sensor along with an ultrasound height sensor above a section of bare ground and then raising and lowering the sensors. The test was then repeated with a forest of fir trees introduced into the same section of ground so that the only variation between the two tests was the introduced foliage. A height estimate was then determined from the time of flight of the first return from each sensor. The results are shown in Figure 5, where the sodar-detected height is compared with the actual height and with the height indication from the ultrasound sensor. For the test above bare ground, both sensors agree well with the actual height. The sodar sensor continues to provide a good estimate of the actual height above ground when the foliage is present, while the ultrasound sensor indicates the height above the tree canopy. The standard error of the post-processed sodar height measurements was less then 0.3 ft for the 30-ft test range above bare ground, and 0.9 ft for the 30-ft test range above vegetation. The attenuation of the sodar return was not significantly affected by the presence of the foliage. This test result provides a clear demonstration of the advantages of the sodar sensor over other sensing modalities with smaller wavelengths, which are less effective at penetrating foliage.

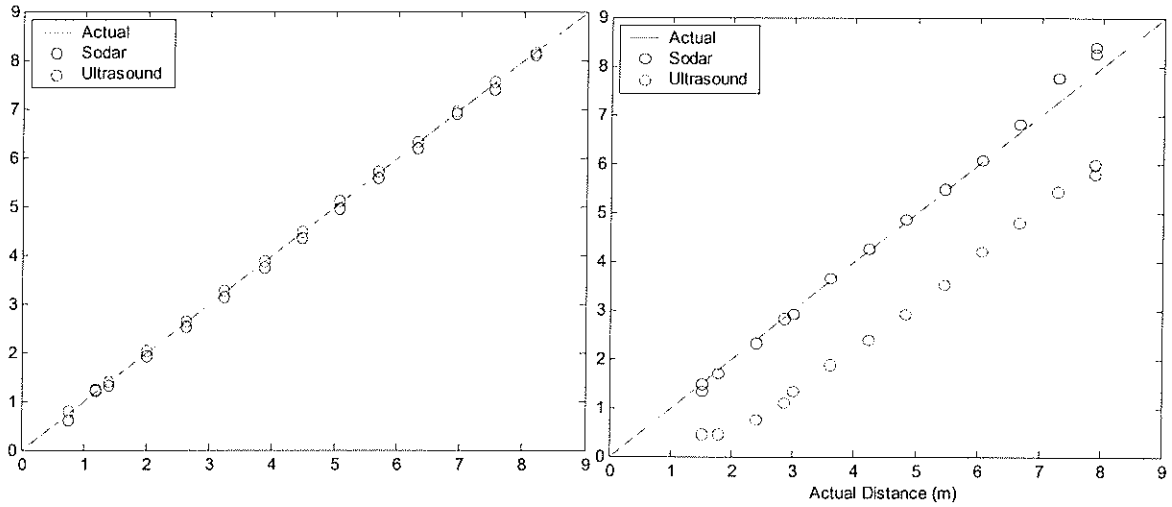

Figure 5. Estimated Height. Comparison of estimated height from the sodar and ultrasound sensors. Results from a test above bare ground on the left and from a test above vegetation on the right. The vegetation does not affect the sodar measurements, but it causes a significant error in the ultrasound measurements.

B. Transmission Angle

The effect of transmission angle on sensor performance was also investigated. For these tests, the sensor was mounted at a height of 65 feet above a grass field and the projection angle was varied from the vertical. The results are shown in Figure 6. The sensor performance is unaffected by variations in the transmission angle of up to 10 degrees from the vertical. Accurate height estimations continue for angles up to 20 degrees from the vertical, although the strength of the return is reduced. At angles greater than 20 degrees, the sensor does seem to measure the slant range to ground implying that it has some forward looking capabilities. The degree of attenuation is dependent on the reflectivity of the ground at increasing slant angles. At an angle of 40 degrees above a grass field, the signal return was almost 25 dB below the vertical value.

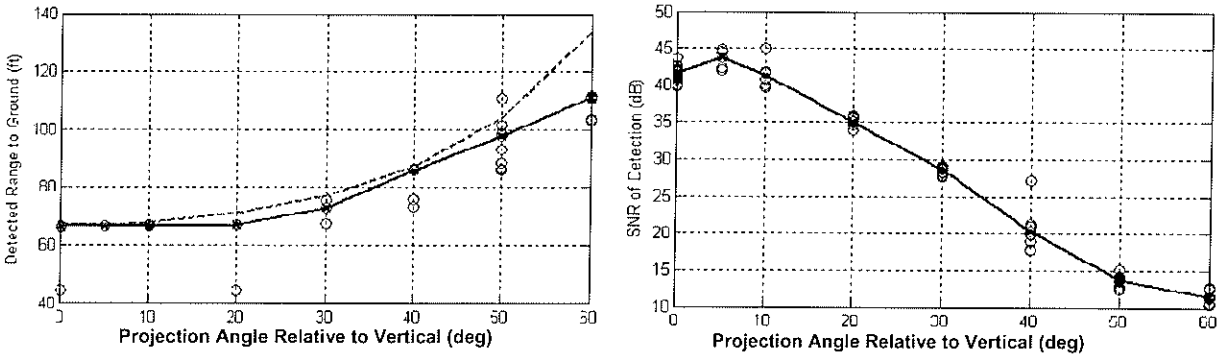

Figure 6. Effect of Transmission Angle on Sodar Sensor Performance. The sensor was operated at a number of angles from the vertical while suspended over a grass field. Range to ground is shown on the left. SNR of the detected returns is shown on the right. Blue circles are detected returns. Black line is the median result. Red line is the boresight slant range to ground at the given angle.

VII. Sensor Field Test Results

The sensor's performance has been characterized in four separate airdrop test series. Two sensor prototypes have survived a total of nine airdrops to date with no major damage. Height data were successfully obtained from seven of these drops. In each of the drops, a data recorder was mounted along with the sensor. The recorder captured the raw microphone signal for post flight analysis. A photograph of the sensor and recorder is shown in Figure 7. The results of each test series are described in the following sections.

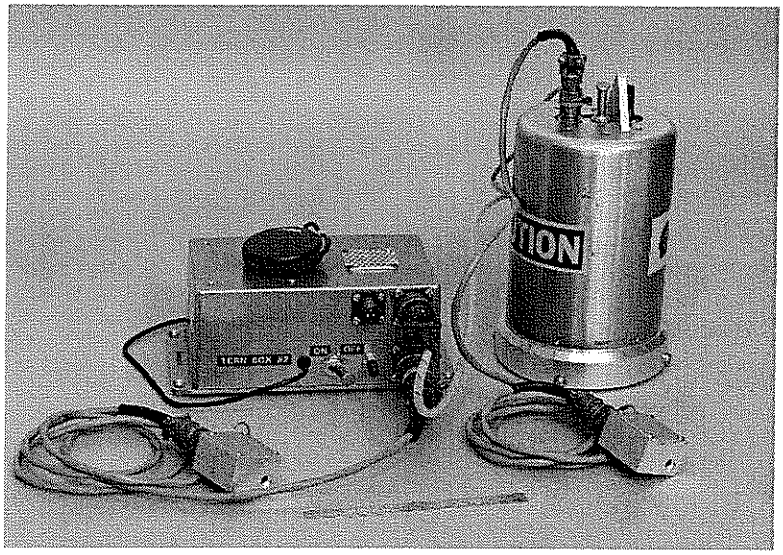

Figure 7. Sensor and Data Recorder Configured for Drop Testing. Both the sensor and recorder are lanyard activated.

A. Para-Flite's Dragonfly System

The first sensor prototype was tested on Para-Flite's 10,000 lb Dragonfly system at Yuma Proving Ground. It was mounted within the AGU, which was suspended above the load. The sensor was controlled by a serial link to the AGU computer. The sensor was carried for two drop tests with releases from C-130 aircraft at 10,000 ft. The AGU failed to power up for the first drop and no data was obtained. Successful soundings were recorded during the second drop along with temperature and pressure data. However, noise from the AGU motors and signal obstruction by the load prevented valid ground returns from being detected during this test. These results prompted the relocation of the sensor to the load and the inclusion of a wireless link to the AGU.

B. MMIST's Sherpa System

A second prototype was tested on a 1,000 lb MMIST Sherpa system at Yuma. The sensor was mounted on the side of the load with a clear view of the ground. A photograph of the sensor mounted on the load prior to the drop was shown earlier in Figure 4. The load was released from a C-130 aircraft at 25,000 feet. The SHS system started sounding at 16,000 ft and temperature and pressure data were recorded from this altitude. Valid ground returns were detected from 400 feet in this test. The results are shown in Figure 8. The sensor noise environment was much quieter than the previous flight and this resulted in good sensor range. The load experienced a severe impact on landing but the sensor survived intact.

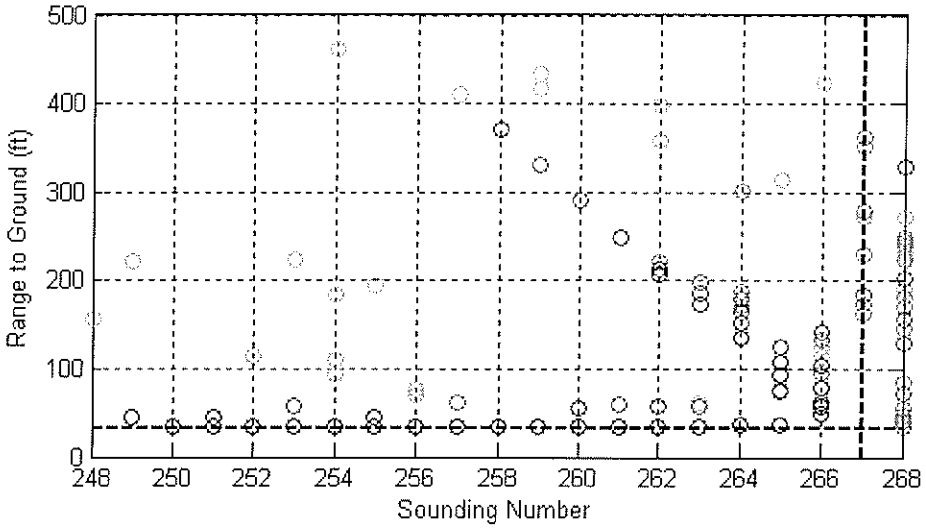

Figure 8. Height Sensor Data From Sherpa Drop.

C. Para-Flite's Microfly System

The final prototype sensor was tested on Para-Flite's 300-lb Microfly system. For the first series of drops, the sensor was mounted at the rear of the load and out of the air stream. This resulted in very low levels of environmental noise and the sensor reported valid height detections at ranges greater than 1,000 ft. The test results are shown in Figure 9. The low noise resulted in an unexpected improvement in the sensor range. This resulted in the ambiguous returns shown in the figure. The adaptive sounding algorithm described in Section IV was introduced to address this problem.

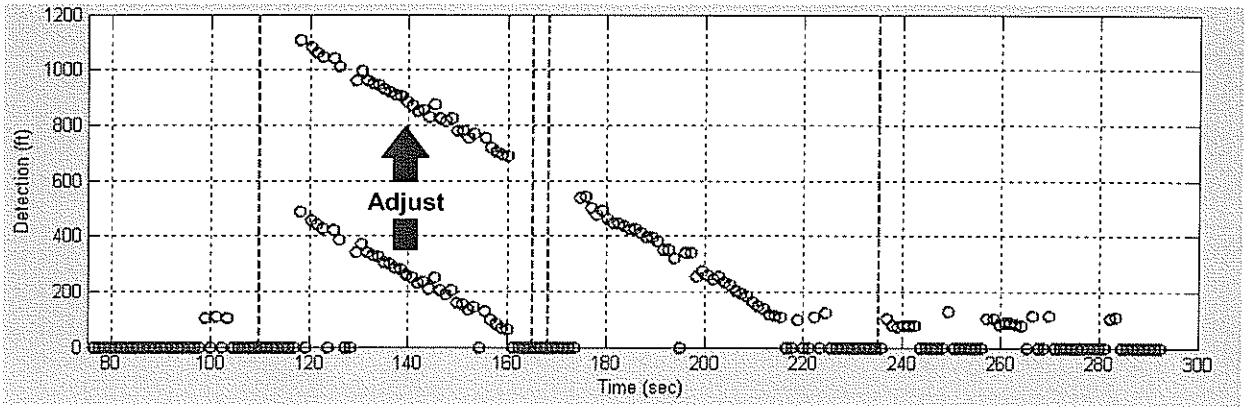

Figure 9. Height Sensor Data From Microfly Drop. Better than expected sensor range resulted in ambiguous height estimates. The incorrect estimates reported by the sensor (shown in red) have been adjusted to show the true height.

The data shown in Figure 9 are from the onboard sensor algorithms. Significant scatter is apparent in the reported estimates. This scatter was later found to be due to an incorrect implementation of the matched filter coefficients. Post processing of the data from the recorder showed improved estimates. The post-processed data from another drop are shown in Figure 10. Pressure altitude is included in this figure. The pressure recordings were referenced to the ground by subtracting an average of the pressure readings recorded after ground impact. The resulting ground-referenced pressure readings were then converted to height estimates. This drop is interesting as the system maneuvered more than in the previous drops. The sodar and pressure estimates agree well throughout the drop. The error between the local pressure altitude and the sodar height estimation is ± 10 ft (95% confidence or 2SD) for this drop. Such an error may easily be attributed to terrain variations along the approach path.

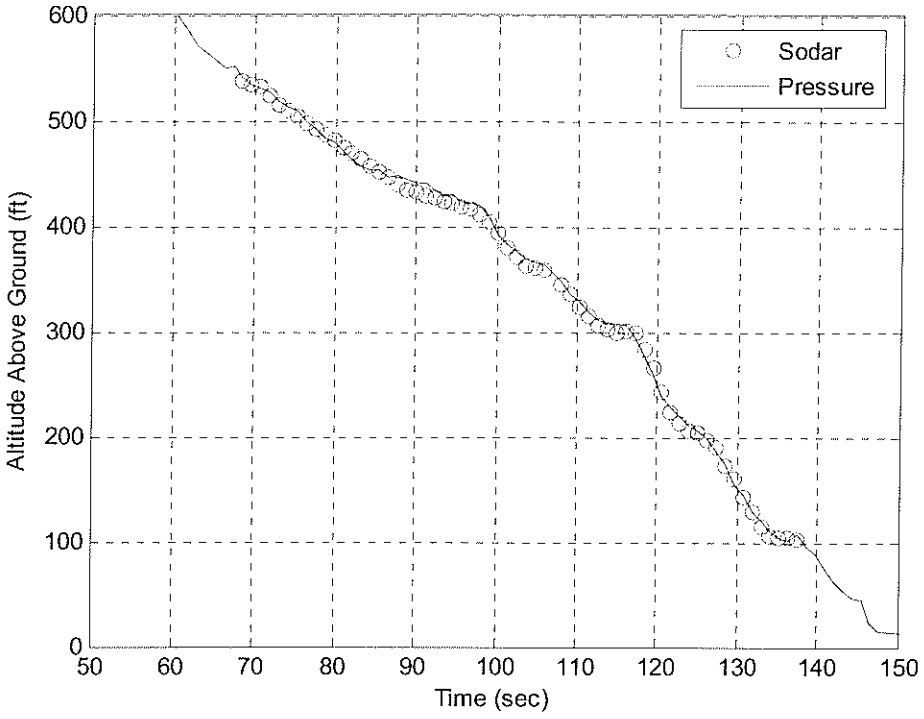

Figure 10. Height Estimates During Final Approach of a Microfly System. Sodar height estimates are compared with pressure altitude referenced to the barometric pressure recorded at the impact point.

Data from the most recent series of tests with the Microfly system are shown in Figure 11. GPS height data were also recorded during this drop. Good agreement between the sodar sensor and the pressure altitude is apparent and both follow a slightly different slope to the GPS height data. The range of the sodar estimates measured during this drop series was significantly less than that measured in the previous series. One possible reason was that the sensor was mounted on the side of the load and exposed to the air stream. Wind generated noise increased the detection threshold and so reduced the range. A 20 dB increase in the threshold would be needed to account for the magnitude of the range reduction. Subsequent road tests conducted with a sensor mounted above a truck demonstrated such an increase in the sensor noise level between side and rear mounted locations. We are currently investigating approached to reduce the effect of self-generated wind noise.

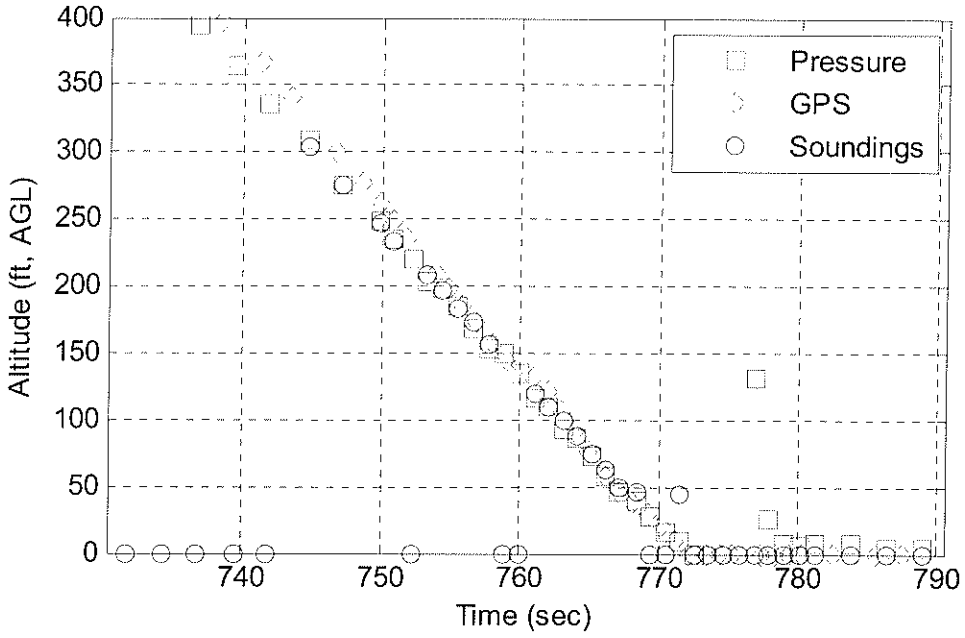

Figure 11. Height Estimates During Final Approach of a Microfly System. Real time sodar height estimates are compared with post-processed pressure altitude referenced to the barometric pressure recorded at the impact point and with post-processed GPS geometric altitude also referenced to the impact point.

VIII. Conclusion

A Sodar Height Sensor has been developed for use with precision airdrop systems. The sensor uses the time of flight of short sound pulses transmitted in the audible frequency range to determine its height above ground. This sensing modality was chosen for its ability to penetrate dust, fog, smoke and ground vegetation and for the availability of relatively inexpensive components. A directional speaker is used to limit the sound broadcast region and the short nature of the pulses result in an innocuous clicking or chirping sound that is inaudible unless one is standing directly underneath the sensor. The sensor is mounted on the payload of the airdrop system in a location where it has a clear view of the ground. It communicates wirelessly with the airdrop system AGU. Height and descent velocity data from the sensor is used by the AGU to time the system's final approach and flare. The result is increased precision of the impact point in the direction of flight and reduced impact velocity. Sensor range is dependent on the noise environment of the airdrop system. Ranges in excess of 1000 ft have been demonstrated when the sensor is mounted in the lee of the load with a clear view of the ground. Sensor accuracies of ±1 foot have been demonstrated in the field.

Acknowledgments

This material is based upon work supported by the U.S. Army RDECOM Acquisition Center, Natick Contracting Division, Natick, MA, under Contract No. W911QY-05-C-0002. The support provided by Para-Flite and Wamore Inc. during airdrop testing is also gratefully acknowledged.

References

Padgham, M., "Reverberation and Frequency Attenuation in Forests—Implications for Acoustic Communication in Animals," J. Acoust. Soc. Am., Vol. 115, No. 1, Jan 2004, pp. 402–410.

Price, M. A., Attenborough, K. and Heap, N. W., "Sound Attenuation Through Trees: Measurements and Models," J. Acoust. Soc. Am., Vol. 84, No. 5, Nov 1988, pp. 1835–1844.

Martens, M. J., "Foliage as a Low-Pass Filter: Experiments with Model Forests in an Anechoic Chamber," J. Acoust. Soc. Am., Vol. 67, No. 1, Jan 1980, pp 66–72.

Ulich, B., Steele, K., McMillin, P., Benney, R., and Bagdonovich, B., "A Sodar Height Sensor for RRDAS," presented at 17th AIAA Aerodynamic Decelerator Systems Technology Conference and Seminar, Monterey, California, May 19-22, 2003.